Proceedings of IDETC/CIE 2006
ASME 2006 International Design Engineering Technical Conferences
& Computers and Information in Engineering Conference
September 10-13, 2006, Philadelphia, Pennsylvania, USA

DETC2006-99752

ELASTIC AVERAGING IN FLEXURE MECHANISMS: A MULTI-BEAM PARALLELOGRAM FLEXURE CASE-STUDY

Shorya Awtar
Precision Engineering Research Group
Massachusetts Institute of Technology
77 Massachusetts Avenue, Cambridge MA
518-577-5500, shorya@mit.edu

Edip Sevincer
Omega Advanced Solutions Inc.
110 8th Street, Troy NY 12180
518-276-8191, sevincer@omegaadvanced.com

ABSTRACT

Over-constraint is an important concern in mechanism design because it can lead to a loss in desired mobility. In distributed-compliance flexure mechanisms, this problem is alleviated due to the phenomenon of elastic averaging, thus enabling performance-enhancing geometric arrangements that are otherwise unrealizable. The principle of elastic averaging is illustrated in this paper by means of a multi-beam parallelogram flexure mechanism. In a lumped-compliance configuration, this mechanism is prone to over-constraint in the presence of nominal manufacturing and assembly errors. However, with an increasing degree of distributed-compliance, the mechanism is shown to become more tolerant to such geometric imperfections. The nonlinear load-stiffening and elasto-kinematic effects in the constituent beams have an important role to play in the over-constraint and elastic averaging characteristics of this mechanism. Therefore, a parametric model that incorporates these nonlinearities is utilized in predicting the influence of a representative geometric imperfection on the primary motion stiffness of the mechanism. The proposed model utilizes a beam generalization so that varying degrees of distributed compliance are captured using a single geometric parameter.

INTRODUCTION

In the design of precision mechanisms, the choice of flexure-based mechanisms over traditional linkage mechanisms is obvious. Lack of friction and backlash in the former provides an exceptional level of precision [1]. However, the biggest drawback in employing a flexure-based design is its reduced range of motion. This may be improved, to some extent, by choosing distributed-compliance over lumped-compliance in the flexure mechanism topology. However, each choice has its own set of distinct advantages and disadvantages. Distributed compliance results in a better distribution of strains, lower stresses, and therefore relatively larger motion ranges. On the other hand, lumped-compliance mechanisms provide excellent stiffness along constraint directions, which leads to improved performance in terms of error motions and stiffness. This tradeoff between range and performance is representative of flexure mechanism design in general [2].

In this paper, we consider the example of a multi-parallelogram mechanism. Fig.1 illustrates three potential embodiments of this mechanism – traditional linkage, lumped-compliance flexure, and distributed-compliance flexure designs. For the flexure-based designs of Fig.1 to be effective motion guides, it is generally desirable to maximize the stiffness along the axial or constraint direction, while keeping the transverse or primary direction stiffness as low as possible. However, any attempt to increase the axial stiffness proportionally by increasing the flexure beam thickness results in a cubic order increase in the transverse stiffness, which is highly undesirable. Therefore, it is common design knowledge to introduce additional parallel beams [3-4], which result in a proportional increase in the axial as well as the transverse stiffness values.

Even though a multi-parallelogram mechanism is desirable for these reasons, mobility remains to be a concern. While it appears reasonable that the linkage mechanism of Fig.1a should have a single degree of mobility, an application of Grubler's criterion [5] reveals zero Degree of Freedom *(5 links, 6 R-joints)*. Although counter-intuitive, it should be recognized that this generic criterion does not take into account the fact that the

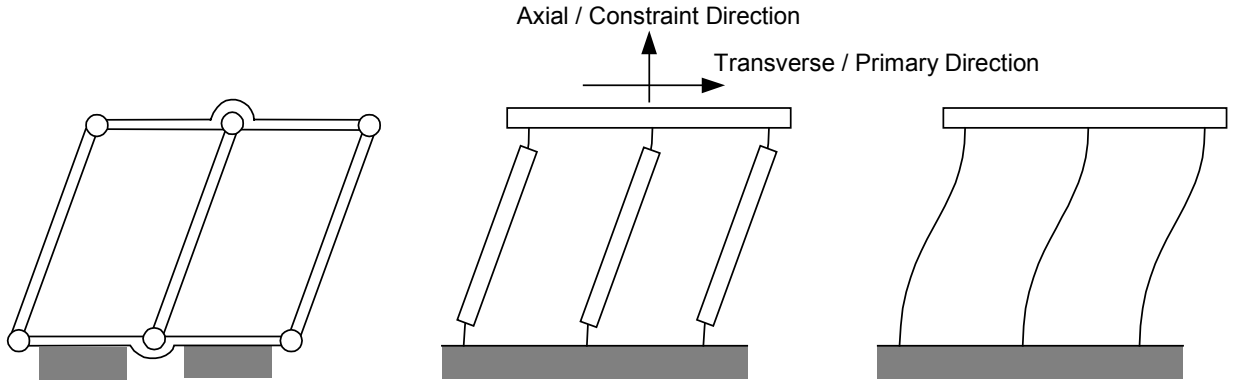

Fig.1 Multi-parallelogram Mechanism a) Traditional Linkage b) Lumped-Compliance Flexure c) Distributed-Compliance Flexure

three links are 'perfectly' parallel. Indeed, with non-parallel links, this mechanism would have no mobility. Grubler's prediction simply serves to make the designer aware that the mobility in this case is sensitive to geometry, and the revolute joints should be made loose enough to accommodate any errors arising from manufacturing or assembly. In other words, this design is prone to *over-constraint*.

In determining the mobility of the lumped-compliance flexure design of Fig.1b, the above conclusions are still valid. Since the lumped-compliance flexure pivots preclude the possibility of 'loose' joints and closely emulate ideal constraints, it becomes very important to maintain tight machining and assembly tolerances. In fact, more than two beams in this design poses a potential over-constraint situation, marked by a dramatic increase in the stiffness along the primary direction in the lack of perfect parallelism. On the other hand, the distributed-compliance version of Fig.1c entails relatively poorer constraint behavior, and therefore provides a higher degree of tolerance to such geometric imperfections. It is shown in this paper that the increase in primary stiffness due to nominal manufacturing errors becomes less significant with increasing degrees of distributed compliance.

The ability of distributed compliance topologies to tolerate potentially over-constrained geometric arrangements owing to their finite stiffness along constraint directions is known as elastic averaging [6]. This is one of the most important attributes of distributed-compliance flexure mechanisms, and allows the designer to depart from the traditional Exact-Constraint design principles [7], which assume ideal constraint behavior. Consequently, elastic averaging has been employed extensively in the conception and design of several novel mechanisms and machines [2,3,6,8].

Two important factors that influence over-constraint and elastic averaging in flexure mechanisms are the nonlinear load-stiffening and elastokinematic effects [2,9]. The latter causes a reduction in axial stiffness in distributed-compliance beams in the presence of transverse displacements, thereby making the mechanism more conducive to elastic averaging. The former affects the transverse stiffness of the constituent beams in the presence of an internal axial forces arising due to geometric imperfections. A simple yet accurate parametric model for nominally generalized beams is used here to capture these nonlinearities in flexure mechanisms ranging from lumped compliance to increasingly distributed-compliance topologies.

GENERALIZED BEAM MODEL [9]

Fig.2 illustrates a nominally generalized beam that is used as the constituent element in the multi-beam parallelogram flexure mechanism discussed subsequently. The beam is shown in a deformed configuration with normalized end-forces and end-displacements. Displacements and lengths are normalized by the overall beam length L, forces by EI/L^2, and moments by EI/L. The two equal end-segments are chosen to have a thickness t and length a_o, and the middle section is thick enough to be considered rigid. The geometric parameter a_o quantifies the degree of distributed compliance: $a_o=1/2$ represents the simple beam with uniformly distributed compliance, while $a_o \rightarrow 0$ corresponds to a lumped-compliance topology.

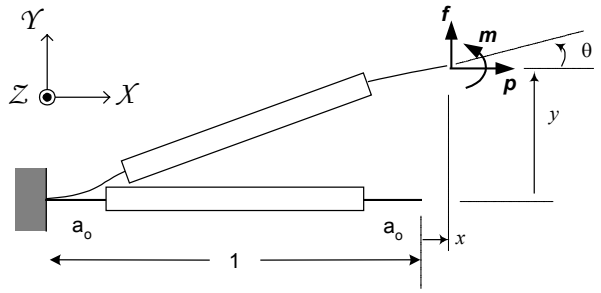

Fig.2 Generalized Beam Flexure

All non-dimensional quantities are represented by lower case letters throughout this discussion. Based on Euler-Bernoulli assumptions and linearized beam-curvature, the following force displacement results may be obtained by considering deformed-state force equilibrium conditions, which capture the contribution of axial load $\boldsymbol{p}$ in the bending moment.

$$\begin{bmatrix} \boldsymbol{f} \\ \boldsymbol{m} \end{bmatrix} = \begin{bmatrix} a & c \\ c & b \end{bmatrix} \begin{bmatrix} y \\ \theta \end{bmatrix} + \boldsymbol{p} \begin{bmatrix} e & h \\ h & g \end{bmatrix} \begin{bmatrix} y \\ \theta \end{bmatrix} \tag{1}$$

$$x = \frac{1}{d}\boldsymbol{p} + \begin{bmatrix} y & \theta \end{bmatrix}\begin{bmatrix} i & k \\ k & j \end{bmatrix}\begin{bmatrix} y \\ \theta \end{bmatrix} + \boldsymbol{p}\begin{bmatrix} y & \theta \end{bmatrix}\begin{bmatrix} r & q \\ q & s \end{bmatrix}\begin{bmatrix} y \\ \theta \end{bmatrix} \quad (2)$$

Expression (1) includes the influence of axial load $\boldsymbol{p}$ on the transverse direction stiffness. The third term in expression (2) represents the elastokinematic effect in a beam, and results in a quadratic drop in axial stiffness with increasing transverse displacements. The coefficients *a*, *b*, *c*, *d*, *e*, *g*, *h*, *i*, *j*, *k*, *r*, *s,* and *q,* are all non-dimensional functionals of the beam shape, and may be expressed as follows for the generalized beam of Fig.2.

$$a = \frac{6}{a_o\left(3 - 6a_o + 4a_o^2\right)} \quad ; \quad b = \frac{\left(3 - 3a_o + 2a_o^2\right)}{a_o\left(3 - 6a_o + 4a_o^2\right)}$$

$$c = \frac{-3}{a_o\left(3 - 6a_o + 4a_o^2\right)} \quad ; \quad \frac{1}{d} = 2a_o\left(\frac{t^2}{12}\right)$$

$$e = \frac{3\left(15 - 50a_o + 60a_o^2 - 24a_o^3\right)}{5\left(3 - 6a_o + 4a_o^2\right)^2}$$

$$g = \frac{a_o\left(15 - 60a_o + 92a_o^2 - 60a_o^3 + \frac{40}{3}a_o^4\right)}{5\left(3 - 6a_o + 4a_o^2\right)^2}$$

$$h = \frac{-a_o\left(15 - 60a_o + 84a_o^2 - 40a_o^3\right)}{5\left(3 - 6a_o + 4a_o^2\right)^2}$$

$$i = \frac{-3\left(15 - 50a_o + 60a_o^2 - 24a_o^3\right)}{10\left(3 - 6a_o + 4a_o^2\right)^2}$$

$$j = \frac{-a_o\left(15 - 60a_o + 92a_o^2 - 60a_o^3 + \frac{40}{3}a_o^4\right)}{10\left(3 - 6a_o + 4a_o^2\right)^2}$$

$$k = \frac{a_o\left(15 - 60a_o + 84a_o^2 - 40a_o^3\right)}{10\left(3 - 6a_o + 4a_o^2\right)^2}$$

$$r = \frac{2a_o^3\left(105 - 630a_o + 1440a_o^2 - 1480a_o^3 + 576a_o^4\right)}{175\left(3 - 6a_o + 4a_o^2\right)^3} \quad (3)$$

$$s = \frac{a_o^3}{175\left(3 - 6a_o + 4a_o^2\right)^3}\left(\begin{array}{l} 105 - 630a_o + 1560a_o^2 - 2000a_o^3 \\ \quad + 1408a_o^4 - 560a_o^5 + \frac{1120}{9}a_o^6 \end{array}\right)$$

$$q = \frac{-a_o^3\left(105 - 630a_o + 1440a_o^2 - 1480a_o^3 + 576a_o^4\right)}{175\left(3 - 6a_o + 4a_o^2\right)^3}$$

Although the above expressions do not include Timoshenko's correction factors, which become increasingly important for small values of a_o, these may easily be incorporated. For the limiting case of a simple beam with a_o=*0.5*, these characteristic coefficients assume the following numerical values.

a	12	*e*	1.2	*i*	-0.6	*r*	1/700
b	4	*g*	2/15	*j*	-1/15	*s*	11/6300
c	-6	*h*	-0.1	*k*	1/20	*q*	-1/1400

Table 1. Characteristic Coefficients for a Simple Beam

In general, based on expressions (3), an optimal beam shape that suits a given application may be selected. Common design objectives include maximizing the axial elastic and elastokinematic stiffness, minimizing transverse elastic and geometric stiffness, minimizing error motions, limiting the stresses, and increasing elastic averaging behavior. Of this list, the last attribute will be considered in the following section.

THREE-BEAM PARALLELOGRAM FLEXURE

A multi-beam parallelogram flexure mechanism comprising of Ground, Motion Stage and three nominally parallel beams is illustrated in Fig. 3. A Free Body Diagram of the Motion Stage is also included. Although simple beams are shown for clarity, the following analytical treatment is valid for the generalized beam discussed in the previous section. While Beams 1 and 2 are assumed perfectly parallel, a parallelism error α is associated with Beam 3. Angle α simulates a typical manufacturing or assembly imperfection, for example, a 1mm parallelism error over 100mm beam length. This provides an estimate of the maximum magnitude of α that is of interest: *0.01*. Consequently, the small angle approximation for sine and cosine functions of α is applicable.

The reason for over-constraint in this mechanism is qualitatively obvious. The arrangement of Beam 1, Beam 3 and the Motion Stage provides a remote center of rotation at C_1 for the Motion Stage [9]. On the other hand, Beam 2, Beam 3 and the Motion Stage result in a remote center of rotation located at C_2. Thus, upon the application of a Y displacement at the Motion Stage, one part of the mechanism works to make the Motion Stage rotate CCW about point C_1 while the other part tries to make it rotate CW about C_2. This obviously imposes conflicting requirements on the Motion Stage resulting in a potential over-constraint. In the presence of Beams 1 and 3 only, the Motion Stage rotation would be approximately given by $y\alpha/w$, whereas Beams 2 and 3, by themselves, would produce $-y\alpha/w$ [9]. Therefore, it is logical to assume that the actual Stage rotation would be bounded as follows.

$$-\frac{y\alpha}{w} < \theta < \frac{y\alpha}{w} \quad (4)$$

Since we are interested in primary motion ranges within ± *0.1*, the Stage rotation should be of the order less than or equal to *0.001*, according to the above estimate. Thus, small angle approximations are justified for the sine and cosine functions of θ as well.

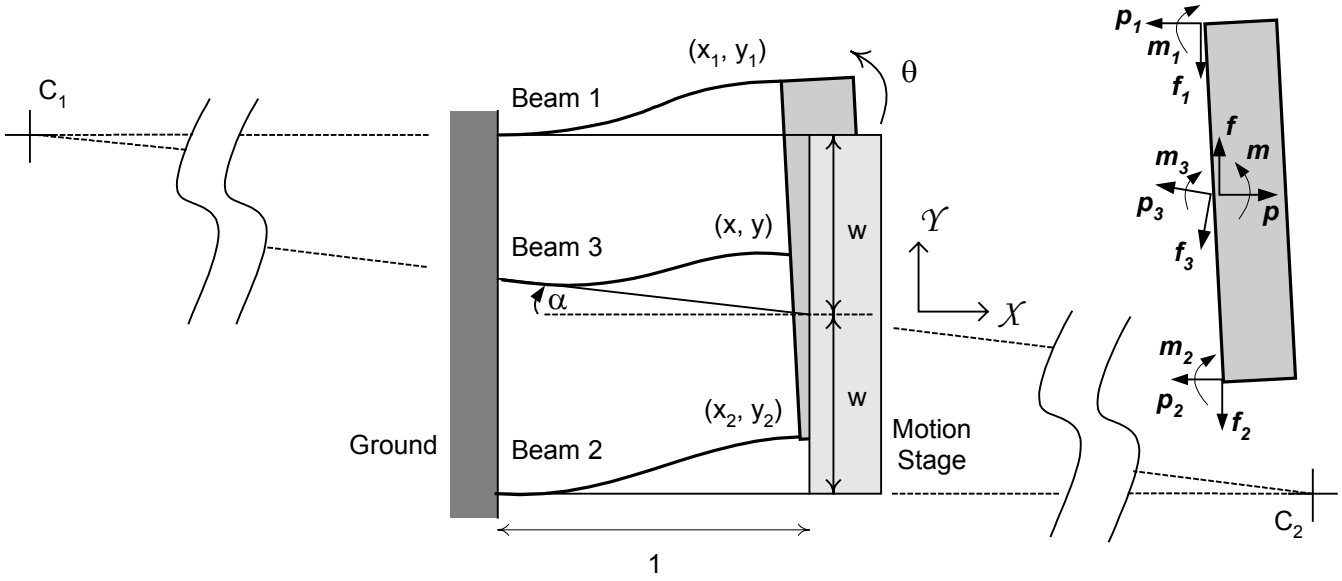

Fig.3 Three-beam Parallelogram Flexure with Geometric Error

Next, we proceed to state the conditions of geometric compatibility between the three beams. The displacements of the individual beam tips are expressed along local coordinate systems aligned with the undeformed configuration of the beam under consideration.

$$x_1 = x - w\theta \quad ; \quad x_2 = x + w\theta$$

$$y_1 = y - w(1-\cos\theta) \approx y$$

$$y_2 = y + w(1-\cos\theta) \approx y \tag{5}$$

$$x_3 = x\cos(\alpha) - y\sin(\alpha) \approx x - y\alpha$$

$$y_3 = y\cos(\alpha) + x\sin(\alpha) \approx y - x\alpha$$

Force-displacement relationships for the three individual beams are simply obtained from expressions (1) and (2). Incorporating the above displacement results and dropping the contribution from θ at appropriate places result in the following expressions.

Beam1:

$$\boldsymbol{f}_1 \approx (a + e\boldsymbol{p}_1)\, y \tag{6}$$

$$\boldsymbol{m}_1 \approx (c + h\boldsymbol{p}_1)\, y \tag{7}$$

$$x - w\theta \approx iy^2 + ry^2\boldsymbol{p}_1 + \frac{\boldsymbol{p}_1}{d} \tag{8}$$

Beam 2:

$$\boldsymbol{f}_2 \approx (a + e\boldsymbol{p}_2)\, y \tag{9}$$

$$\boldsymbol{m}_2 \approx (c + h\boldsymbol{p}_2)\, y \tag{10}$$

$$x + w\theta \approx iy^2 + ry^2\boldsymbol{p}_2 + \frac{\boldsymbol{p}_2}{d} \tag{11}$$

Beam 3: The end loads and displacements in this case are resolved along the local coordinates of the undeformed beam. Furthermore, since the beam length is $1/\cos(\alpha)$, the constitutive relations are slightly modified as follows.

$$\frac{\boldsymbol{f}_3}{\cos^2(\alpha)} \approx \left(a + e\frac{\boldsymbol{p}_3}{\cos^2(\alpha)}\right)\frac{(y + x\alpha)}{\cos(\alpha)}$$

$$\Rightarrow \boldsymbol{f}_3 \approx (a + e\boldsymbol{p}_3)(y + x\alpha) \tag{12}$$

$$\frac{\boldsymbol{m}_3}{\cos(\alpha)} \approx \left(c + h\frac{\boldsymbol{p}_3}{\cos^2(\alpha)}\right)\frac{(y + x\alpha)}{\cos(\alpha)}$$

$$\Rightarrow \boldsymbol{m}_3 \approx (c + h\boldsymbol{p}_3)(y + x\alpha) \tag{13}$$

$$x - y\alpha \approx i(y + x\alpha)^2 + r(y + x\alpha)^2\frac{\boldsymbol{p}_3}{\cos^2(\alpha)} + \frac{\boldsymbol{p}_3}{d\cos^2(\alpha)}$$

$$\Rightarrow x - y\alpha \approx i(y + x\alpha)^2 + r(y + x\alpha)^2\,\boldsymbol{p}_3 + \frac{\boldsymbol{p}_3}{d} \tag{14}$$

Finally, the three force-equilibrium conditions applied to the Motion Stage may be stated as follows.

$$\boldsymbol{f}_1 + \boldsymbol{f}_2 + \boldsymbol{f}_3 - \boldsymbol{p}_3\alpha = \boldsymbol{f} \tag{15}$$

$$\boldsymbol{p}_1 + \boldsymbol{p}_2 + \boldsymbol{p}_3 + \boldsymbol{f}_3\alpha = \boldsymbol{p} \tag{16}$$

$$\boldsymbol{m}_1 + \boldsymbol{m}_2 + \boldsymbol{m}_3 + (\boldsymbol{p}_2 - \boldsymbol{p}_1)w + (\boldsymbol{f}_2 - \boldsymbol{f}_1)w\alpha = \boldsymbol{m} \tag{17}$$

For given end-loads $\boldsymbol{f}$, $\boldsymbol{m}$ and $\boldsymbol{p}$, there are 12 unknowns in the system so far – 9 internal loads, $\boldsymbol{f}_1$, $\boldsymbol{f}_2$, $\boldsymbol{f}_3$, $\boldsymbol{m}_1$, $\boldsymbol{m}_2$, $\boldsymbol{m}_3$, $\boldsymbol{p}_1$, $\boldsymbol{p}_2$, and $\boldsymbol{p}_3$, and three end displacements y, θ and x. These unknowns may be explicitly solved using the 12 equations numbered (6) through (17).

For the purpose of this discussion, we are interested only in the primary or Y direction force-displacement behavior.

Furthermore, to avoid mathematical complexity, an end load comprising of only a transverse force is considered, i.e., $\boldsymbol{m} = \boldsymbol{p} = 0$. This choice simplifies the subsequent calculations without distracting from the final objective of the analysis. Summing equations (8) and (11) yields,

$$x = iy^2 + ry^2\frac{(\boldsymbol{p}_1 + \boldsymbol{p}_2)}{2} + \frac{(\boldsymbol{p}_1 + \boldsymbol{p}_2)}{2d} \tag{18}$$

Equations (12), (16), and (18) may now be used in arriving at the following estimates for the internal axial forces on the beams.

$$\begin{aligned}\boldsymbol{p}_1 + \boldsymbol{p}_2 &\approx \frac{2}{3}\left(\frac{y\alpha}{ry^2 + 1/d}\right)\\ \boldsymbol{p}_3 &\approx -\frac{2}{3}\left(\frac{y\alpha}{ry^2 + 1/d}\right)\end{aligned} \tag{19}$$

These expression are substituted in equations (6), (9), (12) and (15), which may be simultaneously solved to produce the following primary direction force-displacement relationship.

$$\boldsymbol{f} = \left(3a + \frac{2}{3}\alpha^2 d\right)y - \left(\frac{2}{3}\alpha^2 d^2\ r\right)y^3 \tag{20}$$

Primary stiffness follows easily from this expression.

$$\frac{\partial \boldsymbol{f}}{\partial y} = \left(3a + \frac{2}{3}\alpha^2 d\right) - \left(2\alpha^2 d^2\ r\right)y^2 \tag{21}$$

Since the force and displacement values in expression (20) are normalized with respect to EI/L^2 and L, respectively, expression (21) presents a non-dimensional stiffness normalized with respect to EI/L^3. The non-dimensionalized formulation allows us to neglect insignificant terms, wherever appropriate, in arriving at these results. The other two end displacements, x and θ, may similarly be derived but are not immediately relevant to the discussion of this paper.

RESULTS

Expressions (20)-(21) clearly reveal the role of the geometric error α in raising the primary direction stiffness. The stiffness at small displacements increases as a quadratic function of α. Furthermore, the presence and importance of a non-linear term is also evident. This term, which is dependent on the elastokinematic beam coefficient r, results in a displacement-softening behavior. To compare mechanisms with varying degrees of distributed compliance, we can substitute the generalized beam characteristic coefficient expressions (3) in the normalized primary stiffness expression (21), which yields

$$\frac{\partial \boldsymbol{f}}{\partial y} = \left(\frac{18}{a_o\left(3 - 6a_o + 4a_o^2\right)} + \frac{4\alpha^2}{a_o t^2}\right) - \left(\frac{144a_o\left(105 - 630a_o + 1440a_o^2 - 1480a_o^3 + 576a_o^4\right)}{175\left(3 - 6a_o + 4a_o^2\right)^3 t^4}\right)\alpha^2 y^2 \tag{22}$$

This primary stiffness, which is a measure of the mobility of the three-beam parallelogram flexure, is plotted for different values of a_o in Fig.4, assuming $t=1/50$. As expected, the effect of increasing geometric error α has the least impact on stiffness for the simple beam case ($a_o = 0.5$). The increase in primary stiffness becomes more prominent with decreasing degrees of distributed-compliance. Particularly, for small displacements ($y \to 0$), the quadratic increase in stiffness with increasing α becomes more significant for smaller values of a_o. It is also seen that the displacement-dependent non-linear elastokinematic effect helps relieve some of this increase in stiffness with increasing primary displacements. For a given non-zero value of α, the primary stiffness drops as a quadratic function of y. This is simply due to the fact that a larger transverse displacement results in lower axial stiffness of the constituent beams, thereby reducing over-constraint along the primary direction. However, since the elastokinematic effect is a consequence of distributed compliance and reduces with increasing degrees of lumped compliance, the resulting relief in primary stiffness is less significant for smaller values of a_o. These analytical observations reinforce the qualitative discussion of the prior sections.

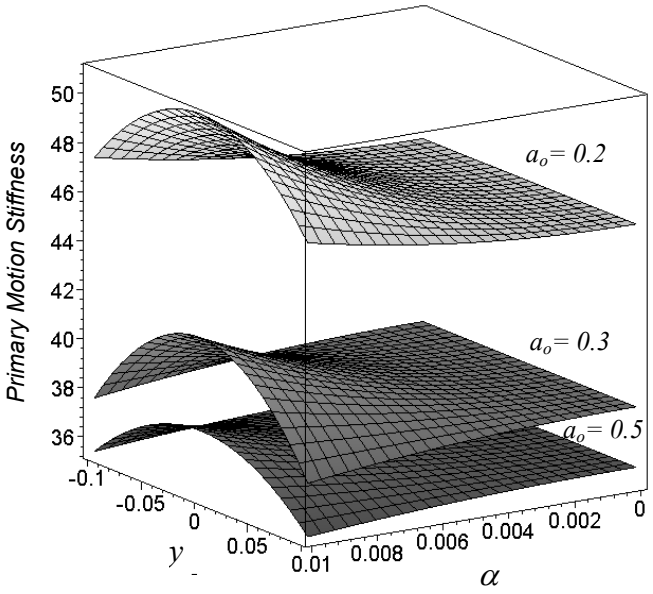

Fig. 4 Normalized Primary Motion Stiffness

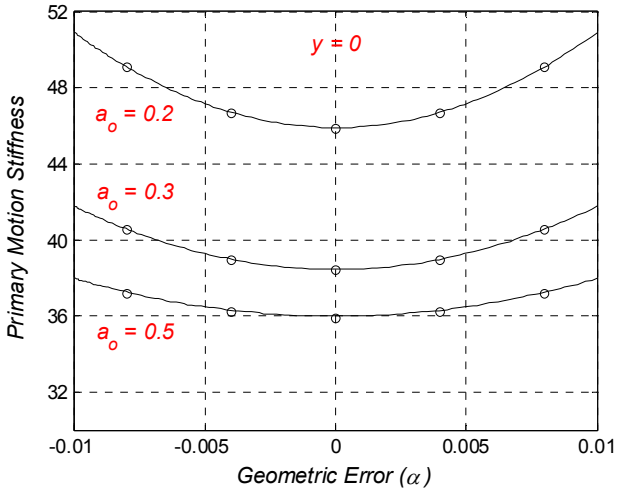

Fig.5 Primary Stiffness (y=0) vs. Geometric Error

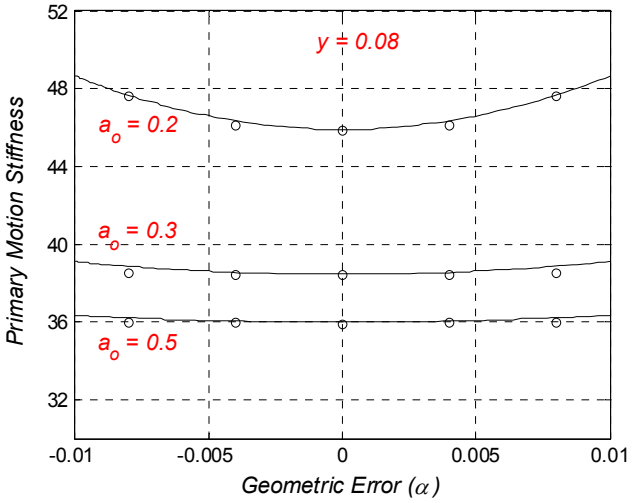

Fig.6 Primary Stiffness (y=0.08) vs. Geometric Error

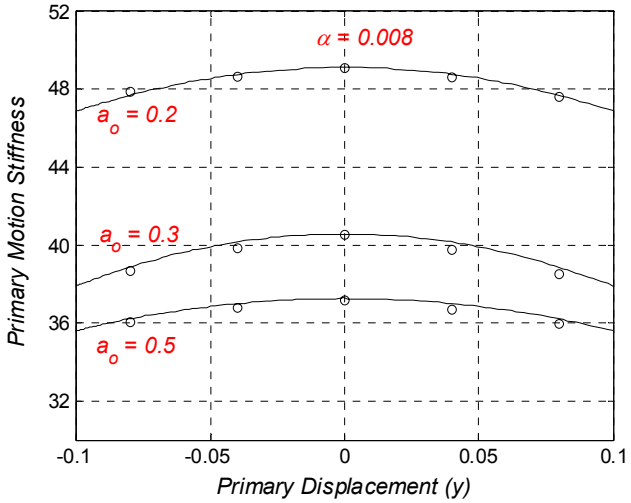

Fig.7 Primary Stiffness (α = 0.008) vs. Primary Displacement

Furthermore, the closed-form analytical expression (22) is validated by means of Finite Element Analysis performed in ANSYS. BEAM4 elements are used with the large displacement option turned on and shear coefficients set to zero. The material assumed is AL6061, and typical values for Young's Modulus (*69,000* N.mm^{-2}) and Poisson's Ratio (*0.3*) are used. Beam length (L) = *250*mm, thickness (T) = *5*mm, and spacing (W) = *75*mm, are chosen for the FEA model. The compliant beam segment length a_o and the geometric error α are varied over typical ranges.

Figures 5 through 7 provide a comparison between the closed-form analysis predications (indicated by solid lines) and FEA results (indicated by circles). The two analyses are found to be in generally good agreement. Fig.5 presents stiffness variation with α, for different degrees of distributed compliance at $y=0$. Not only is the nominal stiffness greater for small a_o, the rate of quadratic increase with α is also higher. For a larger primary displacement, $y=0.08$, the stiffness variation with α are plotted in Fig.6. This figure illustrates the role of the elastokinematic effect in reliving the stiffness caused by geometric imperfection α. Since the elastokinematic effects are more prominent in distributed compliance topologies, the stiffness is restored to a greater extent in these cases as compared to lumped-compliance topologies. The effect of the non-linear elastokinematic behavior is further illustrated in Fig.7. For a given geometric error, $\alpha = 0.008$, the primary stiffness drops with increasing primary displacement because the axial or constraint direction compliance of each beam increases.

CONCLUSION

This paper provides a qualitative discussion and mathematical model for elastic averaging in flexure mechanisms. The tendency of a flexure mechanism to exhibit a significant increase in stiffness along a primary or DOF direction, as compared to the nominal value, in the presence of small geometric imperfections is defined as over-constraint. Special geometric configurations, such as the multi-beam parallelogram flexure, are often desirable for performance improvement, but are susceptible to over-constraint. It is shown here that even though the lumped-compliance topology is beneficial in terms of stiffness characteristics, the distributed compliance topology offers greater robustness against manufacturing and assembly errors, thus avoiding over-constraint. Distributed compliance mechanisms benefit the most from elastokinematic effects in terms of limiting the stiffness increase in an over-constraint prone mechanism.

Although a three-beam parallelogram mechanism and a simple parallelism error were considered here to highlight the concept of elastic averaging, the proposed analysis can be extended to parallelogram mechanisms with more beams, other types of geometric errors, and loading conditions. Similarly, although a specific beam shape generalization has been assumed for the purpose of illustration, the fundamental

concepts discussed in this paper remain relevant for any beam shape.

A preliminary set of FEA results have been presented in this paper, which corroborate the closed-form analysis. A more thorough FEA for several generalized loading conditions is currently in progress. Simple experiments to test the analytical results are also being planned.

Future work includes a rigorous and generic treatment of elastic averaging and its effect on mechanism mobility. Mobility predictions based on Grubler's criterion are clearly more relevant in the case of lumped-compliance mechanism. The analysis presented in this paper illustrates the need for a more appropriate mobility criterion for distributed-compliance flexure mechanisms that recognizes special geometries that are made feasible by elastic averaging. It becomes evident that mobility in such mechanisms is not a binary concept, and that the 'quality' of a constraint relies on potentially varying stiffness values. This investigation leads to a systematic flexure mechanism design philosophy based on 'Approximate' Constraint principles as opposed to 'Exact' Constraint principles.

REFERENCES

1. Jones, R.V., 1988, *Instruments and Experiences: Papers on Measurement and Instrument Design*, John Wiley & Sons, New York, NY
2. Awtar, S., 2004, "Analysis and Synthesis of Planer Kinematic XY Mechanisms", Sc.D. thesis, Massachusetts Institute of Technology, Cambridge, MA (http://web.mit.edu/shorya/www)
3. Bonin, W.A., 2001, "Microactuator Suspension with Multiple Narrow Beams", US Patent 6,282,066
4. Trease, B.P., Moon, Y.-M., and Kota, S., 2005, "Design of Large Displacement Compliant Joints", ASME Journal of Mechanical Design, **127**, pp. 790-798
5. Grubler, M., 1917, *Getriebelehre*, Springer, Berlin, Germany
6. Slocum, A.H., 1992, *Precision Machine Design*, Society of Manufacturing Engineers, Dearborn, MI.
7. Blanding, D.K., 1999, *Exact Constraint: Machine Design Using Kinematic Principles*, ASME Press, New York, NY.
8. Moore, W.R., 1970, *Foundations of Mechanical Accuracy*, Moore Tool Co, Bridgeport, CT.
9. Awtar, S., Slocum, A.H., and Sevincer, E., 2006, "Characteristics of Beam-based Flexure Modules", ASME Journal of Mechanical Design, *in press*